Pergamon

Bioorganic & Medicinal Chemistry, Vol. 5, No. 9, pp 1751–1773, 1997

PII: S0968-0896(97)00145-4
0968-0896/97 $17.00 + 0.00

A Molecular Modeling Analysis of the Binding Interactions Between the Okadaic Acid Class of Natural Product Inhibitors and the Ser–Thr Phosphatases, PP1 and PP2A

Carla-Maria Gauss,[a] James E. Sheppeck, II,[a] Angus C. Nairn[b] and Richard Chamberlin[a,*]
[a]*Department of Chemistry, University of California at Irvine, Irvine, CA 92697, U.S.A.*
[b]*The Rockefeller University, 1230 York Avenue, New York, NY 10021, U.S.A.*

Abstract—We have proposed computer-generated models of the catalytic subunits of the serine–threonine protein phosphatases PP1 and PP2A complexed with their endogenous substrate phospho-DARPP-32, and several known naturally occurring inhibitors. This study is part of an overall effort to elucidate the signal transduction pathways in which PP1 and PP2A may play an important role. © 1997 Published by Elsevier Science Ltd.

Introduction

Reversible phosphorylation of the 'molecular switches' dopamine cyclic AMP-regulated phosphoprotein (DARPP) and its isoform inhibitor-1 (I-1) catalyzed by protein kinase A and the protein phosphatases PP1 and PP2A is currently the subject of many investigative efforts. There is a structurally diverse group of natural toxins, including okadaic acid, calyculin, microcystin LR, and tautomycin, that exert their cytotoxic effects by inhibiting PP2A and/or PP1, thereby preventing the dephosphorylation of DARPP and disrupting the normal signaling pathways. Interestingly, despite the dissimilarities of their structures, these compounds are competitive inhibitors; i.e., their PP1/PP2A binding sites overlap. A recently published X-ray structure of a PP1-microcystin LR complex provides a unique opportunity to explore binding interactions of all of these inhibitors with both PP1 and PP2A, and potentially to develop new selective inhibitors based on these natural products.

An Approach to the Prediction of Toxin Binding Conformations

The working hypothesis

In attempts to propose models for how the okadaic acid class of inhibitors interacts with the same binding site on PP1 or PP2A, one would certainly exploit the common themes or structural motifs among the inhibitors. Recently, a molecular modeling comparison of microcystin, nodularin, calyculin, and okadaic acid has provided some evidence for a common pharmacophore among this group.[1,2] The authors argue that the criteria for determining whether a compound may inhibit PP1 or PP2A based on these structures are: there must be an acid such as carboxylate or phosphate; there must be a hydrophobic tail; and there may or may not be a portion of the molecule that mimics a peptide for binding to a phosphatase peptide recognition domain. Our working hypothesis is that the microcystins, nodularins, okadaic acid, calyculin, tautomycin, and even cantharidin are sophisticated mimics, not only of the binding domain in the vicinity of phosphothreonine-34 of DARPP (and/or I-1), but of one another. We have analyzed the PP1-microcystin X-ray structure, in conjunction with the structure–activity data presented previously,[3] to sketch a composite picture of the prerequisites necessary for a potent phosphatase inhibitor.

The acidic group. All of the inhibitors except for thyrsiferyl-23-acetate contain a phosphate or apparent (di)carboxylate group. The PP1 dinuclear Mn^{2+}/Fe^{2+} metal active site that binds to the phosphorylated serine and threonine of substrates is occupied by microcystin's isoglutamic carboxylate and an intervening water molecule. Ubukata et al. have conjectured that the acidic moieties of okadaic acid and tautomycin may mimic the phosphorylated Ser–Thr of natural substrates.[4] Although conceivable, it is difficult to imagine that the phosphate of calyculin does not also bind this site. In an unrelated example, aryl malonates (1,1-dicarboxylates) act as phosphotyrosine mimics to inhibit SARC homology domains, and we believe that the 1,2-dicarboxylates of hydrolyzed tautomycin and cantharidin, and the α-hydroxy carboxylate of OA, can also serve as phosphate mimics in the binding site of PP1/2A (Fig. 1). This notion is supported experimentally since the monopropyl ester of microcystin, the methyl ester of OA, the cyclic imide of cantharidin, and DARPP32 mutants that have replaced the phosphothreonine with an aspartate, are substantially compromised inhibitors. Cantharidin is also a competitive inhibitor with pyrophosphate, which is compelling evidence

that it is binding the active site since it bears virtually no other functionality. Endothall thioanhydride is the most potent analogue of cantharidin presumably because the thiolate is superior to carboxylate as a ligand for coordination to either the Fe or Mn metal in the active site. Removal of the α-hydroxyl substituent of OA also compromises its inhibition of PP1/2A. We also cannot exclude the possibility that the carboxylic (di)acid moieties of cantharidin, okadaic acid, and tautomycin may act as transition-state mimics of a hydrolyzing phosphate.

We believe that the diacid forms (or their salts) of cantharidin and TM are the active PP-inhibitory forms rather than the anhydrides themselves. Although there is a discrepancy in IC_{50} between the anhydride and diacid of these two molecules, this might just be an experimental artifact due to hydrolysis or solubility problems.[5] However, another possibility exists: the anhydride is hydrolyzed by the phosphatase itself, rather than by bulk water. If both metals lost their *m-oxo*-bridging water (or OH^-) on initiating the anhydride hydrolysis, they would become more Lewis acidic and bind the resultant carboxylates more strongly.

On inspection, the diacids of cantharidin and tautomycin are functionally more analogous to the phosphate in the X-ray structure than are the microcystin and okadaic acid carboxylates since they can form strong electrostatic interactions with the Arg-rich active site. For the same reason, it is also likely that DTX4—an ester of okadaic acid that should have low activity—retains good inhibition of PP1/2A because its polysulfate terminus likely interacts favorably with the active site arginines.

Thus, we predict that the acidic group (in the form of its conjugate base) of each of the inhibitors occupies the phosphate binding site of PP1/2A, which provides an important anchor-point for orienting the inhibitors for the docking studies undertaken.

The methyl substituent. A striking feature of these inhibitors (particularly tautomycin, OA, cantharidin, and calyculin) is that in each case there is a methyl group directly adjacent to the carboxylate or phosphate. If the acidic groups are indeed situated in the active site of the enzyme, this apparently conserved methyl group might represent a phosphorylated threonine mimic. It is known that phosphothreonine-containing peptides are significantly better substrates for PP2A than the analogous phosphoserine peptides, and Greengard and coworkers have shown that replacing phosphothreonine in truncated DARPP with phosphoserine dramatically diminishes its inhibition of PP1.[6,7] These data argue strongly for enhanced binding of inhibitors/substrates to PP1 and PP2A due to (i) a methyl binding site in the enzymes proximal to the acidic binding site or, (ii) conformational restriction induced by the methyl group that preorganizes their structure. It may thus be no coincidence that removal of the two methyl groups from cantharidic acid decreases inhibition 14-fold.

Figure 1 shows a modeling comparison of the excised acidic portions of OA, TM, cantharidin, calyculin, and phosphoDARPP. Superimposition of the oxyanions (charges were arbitrarily assigned) of the carboxylates with those of the phosphates in calyculin and DARPP, allows for good overlap of the OA α-hydroxyl, cantharidin and the second carboxylate of TM, and the phosphoric ester hydroxyl of calyculin and of DARPP. We believe that the relative position of the proximal methyl substituent (lower left, as shown) is not coincidental, but present in most of the inhibitors to exploit extra binding energy via a methyl binding site in PP1/2A. This site also appears to be present in PP2A because phosphothreonine-containing substrates are dephosphorylated faster than phosphoserine-containing substrates. Homologous calcineurin, however, dephosphorylates both types of substrate at comparable rates.[6,8]

The hydrophobic/peptidomimetic segment. All of the inhibitors (save cantharidin) have a hydrophobic terminus that is important for potent inhibition of PP1/2A. The published structure appears to confirm our original (pre-X-ray) belief that the intriguing conserved Adda side-chain of microcystin is a peptide isostere mimicking the hydrophobic sequence (AMLF) of amino acids 36–39 of DARPP. In the complex, the Adda side-chain of microcystin resides in a cleft that is proposed by the authors to accommodate the AMLF residues of phospho-

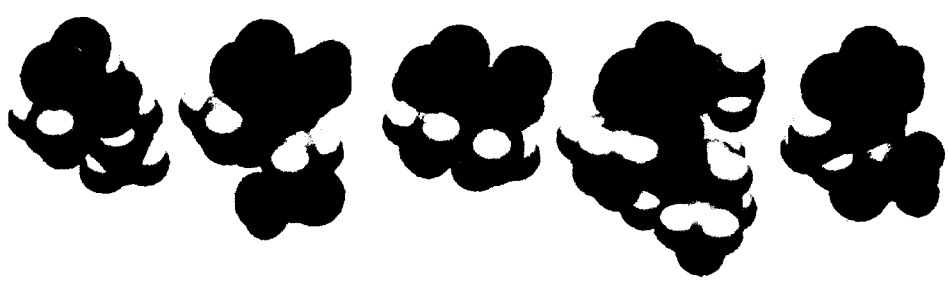

Figure 1. The acidic groups of several OA-class inhibitors with proximal methyl substituent(s).

DARPP. Calyculin also seems to have a peptidomimetic chain. In fact, one could argue that the macrocycle of microcystin and the spiroketal of calyculin mimic the proline-induced turn in DARPP. The terminal spiroketals of OA and TM are also highly hydrophobic and like microcystin, nodularin, and calyculin, appear to be appropriately disposed to interact with the aforementioned hydrophobic binding site. Interestingly, since thyrsiferyl-23-acetate contains only the hydrophobic functional group, and cantharidin contains only the acidic functional group, both of these inhibitors are 10^4 times less potent than the other OA inhibitors that make use of both. In fact, calyculin, TM, OA, and the cyclic peptides can be thought of as a tethered combination of cantharidin and thyrsiferyl acetate. This idea is fully consistent with the fact that the hydrophobic half of OA is still PP-inhibitory albeit not as potent as OA itself.

Previous conformational analyses

In 1989, Uemura and Harata proposed that okadaic acid forms a flexible cavity via an internally H-bonded conformation based on NOE NMR data that were similar to the X-ray structure of the *o*-bromomethyl ester of OA[9,10] and proved consistent with later SAR data.[11–13] Using molecular mechanics, Quinn et al.[1] arrived at a similar conclusion for okadaic acid, which was also later corroborated by Murata's analysis using long-range carbon–proton coupling constants in $CH_3OD/CDCl_3$ under approximated 'physiological conditions' (0.1 M $NaOD/D_2O$) followed by computational refinement.[14]

Similarly, conformational analysis of the diacid of tautomycin was investigated using solution NOE NMR data and NMRgraf [DISCOVER/INSIGHT-(Biosym)].[5] This 'molecular shape analysis' was shown to bear close resemblance to the OA structure above by superimposition of the acids and respective spiroketals exactly 180° opposite to the alignment of OA and TM earlier proposed by MacKintosh and Klumpp in 1990.[15] The equilibrium of TM between the anhydride and diacid in H_2O has been emphasized such that the analogy between the TM and OA acids is reasonable.

In regard to the cyclic peptide inhibitors, Lanaras et al. published a computer modeling analysis comparing microcystin-LR to nodularin-R. Quinn, Fujiki, and co-workers later revised this comparison using molecular mechanics to calculate the global minima of both inhibitors.[2,16] Their modeling analysis was later expanded to include okadaic acid (which was conformationally similar to earlier findings as mentioned above) and calyculin-A; the latter also formed an internally hydrogen-bonded conformation analogous to that found in the X-ray structure.[17] The calculated cyclic structures of OA and calyculin were predicted to mimic the macrocyclic structures of the microcystins and nodularins culminating in a pharmacophore model for these members of the OA-class that consists of a conserved acidic group, two potential hydrogen-bonding sites, and a nonpolar side-chain.[1] Although the computationally generated model proposed by Quinn is consistent with much of the available SAR data, he presents no additional experimental evidence to substantiate it.

The published conformational studies reviewed above offer comparisons of energetically reasonable conformations of each inhibitor. However, since the three-dimensional structures of the phosphatases were not known at the time, modeling alone does not adequately approximate the most important structure of all: the *bound* conformation of each inhibitor. It is really only within the PP1 and PP2A catalytic subunit binding sites themselves that the competitive inhibitors must be able to achieve structural congruence with one another. The same dilemma applies to 'real' conformations; that is, those that might be determined experimentally in solution or in the solid state. Thus, while it may be reassuring to find good overlap among calculated structures of competitive inhibitors, there is no computational way to know whether they represent those actually responsible for the observed inhibition; i.e., the bound forms, without knowing the structures of the PP1 and PP2A binding sites.

Calculation of the Structures of Phosphothreonine, DARPP-32, and Calyculin with PP1

The key strategy in developing binding models for the phosphatase inhibitors containing a phosphate group was to identify an initial low-energy conformation for the simple substrate phosphothreonine; and then, to dock the phosphate groups of the inhibitors in a similar orientation prior to minimization. Phosphothreonine was chosen over phosphoserine to formulate this prototype for two reasons: first, phosphothreonine is the residue in DARPP-32 that occupies the binding site; second, phosphothreonine contains a β-methyl substituent, and our hypothesis suggests that the methyl groups proximal to the phosphate or carboxylate groups in the inhibitors may serve as mimics for the methyl group in phosphothreonine. Further rational development of a binding model should take into account the appropriate structural features of the enzyme which may be responsible for catalysis.

As previously mentioned, Goldberg et al.[18] published the structure of rabbit PP1 cocrystallized with the peptide inhibitor microcystin-LR; soon after, Barford's group published the structure of human PP1 cocrystallized with tungstate bound in the active site.[19] Taken together, along with PP mutagenesis studies, these crystal structures have immensely clarified how PP1/2A dephosphorylate substrates and how they might be regulated; and they show specifically how microcystin acts to inhibit the enzymes at the molecular level.

Comparison of the primary sequence of PP1/2A/2B shows that all of the metal ligands are strictly conserved (PP2B has Fe^{2+} and Zn^{2+} metal ions in the active site) and many of the amino acids in the vicinity of the active site are likewise conserved. Mutation of any of these amino acids is highly deleterious to the catalytic activity of the PPs. In close proximity to the active site is a critically important flexible peptide chain known as the β12–β13 loop. As briefly discussed below, this loop appears to be the only flexible part of the enzyme and not only obscures the active site to exclude phosphoTyr-containing substrates, but also appears to contact all of the OA-class inhibitors examined to date as well as DARPP, I-1, and I-2.

Inspection of PP1's topology shows that the enzyme contains 10 α-helices and three β-sheets. The active site contains a dinuclear metal complex of an Fe^{2+} ion at the primary metal site (M1) and a Mn^{2+} ion at the secondary site (M2) in a shallow groove on the surface of the protein. The metals were unambiguously determined to be in the active site from the Barford structure of PP1 and the published structure of PP2B because they are coordinated to tungstate and phosphate, respectively.

Plausible ligand geometries about the metal ions in the active site have been deduced by analysis of pertinent data from the X-ray crystal structures. Barford and co-workers describe the coordination at M1 in their crystal of the free enzyme as a trigonal pyramid.[19] The ligands believed to coordinate M1 are a water molecule and the residues Asp64, His66, and Asp92. The authors speculate that Tyr272 may also coordinate to M1 which would "convert the metal ion geometry to a square pyramid."[19] For the metal ion at M2, the ligand geometry is purportedly square pyramidal. Ligating residues are Asp92 (shared with M1), Asn124 (through the amide carbonyl), His173, and His 248; in addition, there appears to be a coordinating water molecule. Kuriyan and co-workers did not publish a crystal structure of the uncomplexed enzyme, but they postulate comparable geometries around the metal ions.[18] In their proposed structure, the environment around M1 is thought to be square pyramidal with Asp64 at the apex, and Asp92, His66, and two water molecules comprising the base of the pyramid. For M2, they propose a 'distorted' trigonal bipyramid with Asp92 and His248 as the axial ligands, and Asn124, His173, and a water molecule as the equatorially coordinating ligands.

It has been suggested that the catalytic mechanism of action of the protein phosphatases involves "metal-ion mediated hydrolysis of the substrate by a metal-activated (OH^-) water molecule."[19] The following theories are cited: the metal ions orient the phosphate favorably for the approach of a nucleophile; the metal atoms inductively activate the phosphorous atom making it more susceptible to nucleophilic attack; the metal ions may assist hydrolysis by coordinating a potentially nucleophilic water molecule bringing it in close proximity with the bound phosphate.[19] Additionally, the residue His125 may serve as a general acid (charge stabilized by Asp95) which protonates the phosphate ester making it susceptible to hydrolysis by the water molecule. Hydrolysis of the phosphate triggers release of the substrate and regeneration of the catalyst by replenishing the active site water and the His125 general acid. The catalytic mechanism of these PPs seems to be at the 'lock and key' extreme of the spectrum because binding of phosphate to PP1 induces almost no conformational change in the enzyme; the β12–β13 loop seems to be the only flexible part of the protein.

The structure of the catalytic domain of PP1 used in our simulation was taken directly from the X-ray crystal coordinates kindly provided to us by Kuriyan and co-workers.[18] A preliminary approximation for the position of the phosphate group in the binding site was made based on the data from the X-ray structure of the phosphate analogue tungstate bound with the catalytic subunit of human $PP1_{\gamma 1}$ as described by Barford and co-workers.[19] In this structure, "two tungstate oxygen atoms are coordinated at the dinuclear metal site" with oxygen–metal distances of 1.8 and 1.9 Å.[19] One remaining oxygen is doubly hydrogen bonded to Arg221 (in turn hydrogen bonded to Asp208) and the amide nitrogen of Asn124, and the other is doubly hydrogen bonded to Arg96 and the invariant His125. After phosphate complexation, the coordination at the metals may be octahedral if an additional water molecule can be presumed to act as the sixth ligand.[19]

The next step was to minimize and compare several different starting conformations for phosphothreonine in which the phosphate group satisfied the docking prerequisites in the binding site; that is, initial distance measurements were made between the phosphate oxygens and the metal ions using the corresponding distances from the X-ray structure of tungstate bound to PP1.[19] Since the Biosym forcefields are currently not parameterized to handle transition metal ions, the metal ions were excised from the model structure after the initial docking. Instead, the phosphate group was constrained to the metal ligands by setting distance restraints from the phosphate oxygens to the metal-coordinating atoms in the metal ligands. Subsets of the protein were defined so that residues within 7 Å of phosphothreonine were allowed to relax while the rest of the protein was held fixed. This distance was chosen to encompass all of the amino acid side-chains known to contact microcystin and tungstate in their respective X-ray structures. By defining a subset for conformational searching containing only the residues implicated in catalysis, there is minimal distortion of the protein tertiary structure since it is known not to be greatly perturbed by binding tungstate.[19] The preliminary structures were then subjected to minimization and dynamics optimization using the Discover_3 Module in the Insight 95.0 program. Minimizations were performed over 20,000 steps reaching a convergence of 0.01 kcal/mol Å using the steepest descents method to a convergence of 10 kcal/mol Å followed by the conjugate

(a)

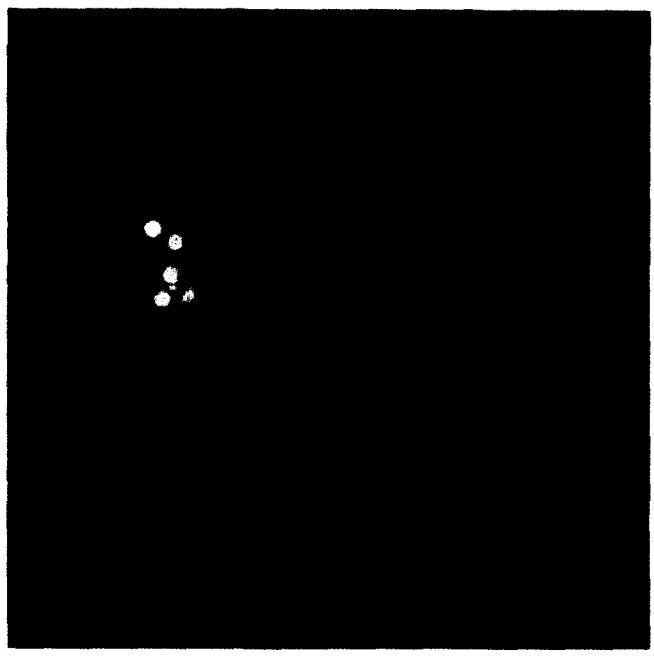

(b)

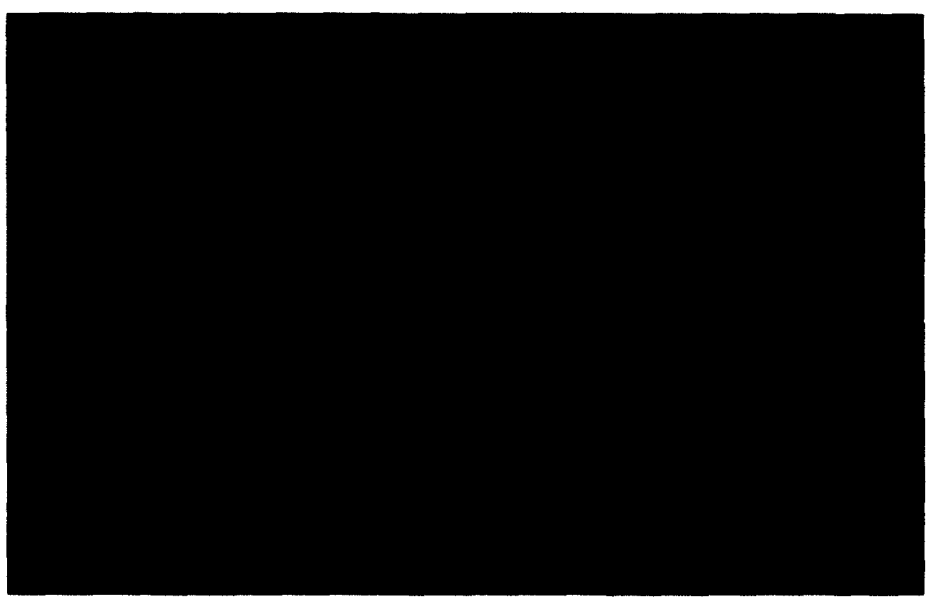

Figure 2. (a) Side view of phosphothreonine bound to the active site of PP1. The phosphothreonine molecule is represented in CPK mode and color coded by atom type: carbon, gray; nitrogen, blue; oxygen, red; hydrogen, white. PP1 is in blue. Metal ions are shown as spheres in fuchsia. (b) Stereo view of phosphothreonine with the active site contacting residues of PP1. The phosphothreonine molecule is color coded by atom type as for 2(a). PP1 residues are represented in gold. The metal ions are shown as spheres in fuchsia.

gradients method to reach final convergence. Dynamics simulations were then performed at 300 K over a timestep of 5000 fs. The five lowest energy structures were then subjected to another minimization using the same parameters as before (see the Materials and Methods section for further details). The lowest energy conformation found is shown in Figure 2. Analysis of this model reveals a favorable hydrophobic interaction between the methyl group of phosphothreonine and His248; this could be the contact that is preserved between the enzyme and the inhibitors. The phosphate

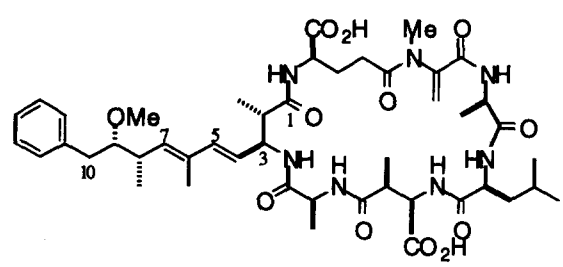

Microcystin-LA
(blue-green algae)

group is held in the active site by interactions with the metal ions, His125, Arg96, Arg221, and Tyr272.

Our first goal was to model residues 31–39 (Arg-Arg-Pro-PThr-Pro-Ala-Met-Leu-Phe) of the endogenous inhibitor DARPP-32 with PP1. We selected these residues for the model since their side-chains are structurally comparable to microcystin and flank the key residue, phosphothreonine-34, which has been shown to be critical for potent inhibition of PP1.[6] Additional residues of DARPP would extend far beyond the microcystin binding site and were therefore not considered for lack of information about their possible binding modes. The preliminary structure of DARPP was constructed in the Bioplymer Module of the InsightII program developed by MSI of San Diego (see Materials and Methods). Based on our proposal that the Adda side-chain of microcystin is a peptidomimetic for residues 36–39 of DARPP-32 (Pro-Ala-Met-Leu-Phe), we overlaid these residues of DARPP with Adda in two orientations for initial conformational searching. In the first orientation, we superimposed the carboxylate residue of microcystin with the phosphate group of DARPP and the following three atoms of Adda with atoms in residues 36–39 of DARPP: the C6-methyl carbon of Adda with the Ala methyl carbon of DARPP, the Adda C8-methyl carbon with the β-methylene carbon of the Met residue of DARPP, and the Adda methoxy carbon with a methyl carbon of the Leu residue of DARPP. In the second orientation, we superimposed the C2-methyl carbon of Adda with the methyl group carbon of Ala in DARPP, the C6-methyl carbon of Adda with a methyl group carbon of Leu in DARPP, the C4–C5 alkene of Adda with the Met-Leu amide bond of DARPP, and the phenyl ring of Adda with the phenyl ring of Phe in DARPP. These structures were then subjected to minimization performed over 20,000 steps (this was found to be the optimum number of steps to reach the lowest energy structures) and reaching a convergence of 0.01 kcal/mol Å using the steepest descents method followed by the conjugate gradients method to reach final convergence. Dynamics simulations were then performed at 300 K over a timestep of 5000 fs. The five lowest energy structures were then subjected to another minimization using the same parameters as before.

We then used our working hypothesis, previously delineated, as our guide for docking the model structures with PP1. To begin, the phosphothreonine residue of DARPP was superimposed with the calculated model of phosphothreonine coordinated to the metal ions. We used the position of Adda in the hydrophobic pocket as established in the X-ray structure as a guide for docking residues 36–39 of DARPP. Distance restraints between these residues of DARPP and the hydrophobic residues which contact Adda were set based on the X-ray structure. Kuriyan and coworkers[18] suggest that there is an 'acidic' groove consisting of aspartate and glutamate residues which may serve to bind substrates or inhibitors with basic side-chains. Therefore, the arginine residues at the amine terminus of the inhibitor were docked and restrained (to 2.5 Å) such that favorable contacts might be made with Glu256, Glu252, Asp210, and Asp212. The fact that increasing the number of *N*-terminal arginines in this sector increases the rate of dephosphorylation by PP2A may be indicative that these residues are key to binding.[20] At this stage, four initial conformations of the docked inhibitor were deemed satisfactory for proceeding with minimization and dynamics. These four conformations differed slightly in rotation of bonds and proximity to the active site residues. An additional structure of DARPP was docked into the catalytic site under the same general guidelines as the others, but without distance restraints for the calculations. Subsets of the protein were defined so that the residues 8 Å around DARPP (this distance was chosen so that all of the active site residues which contact microcystin would be included in the calcula-

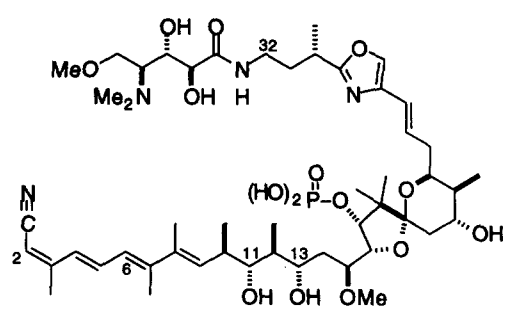

(-)-Calyculin
(sponge)

Table 1. Effects of OA-class inhibitors on wild-type and mutant PP1[20]

	IC_{50} (nM)			
PP1	**Microcystin-LR**	**Okadaic acid**	**Calyculin-A**	**S-DARPP-32**
Wild-type	0.023	45	0.45	115
E275R	0.0091	48	0.4	2.2
C127S	0.56	78	2.2	250
Y272F	0.8	1150	48	310
D208A	4.9	>5000	>500	4.2
R96A	35	260	58	640
R221S	29	>5000	>500	960

(a)

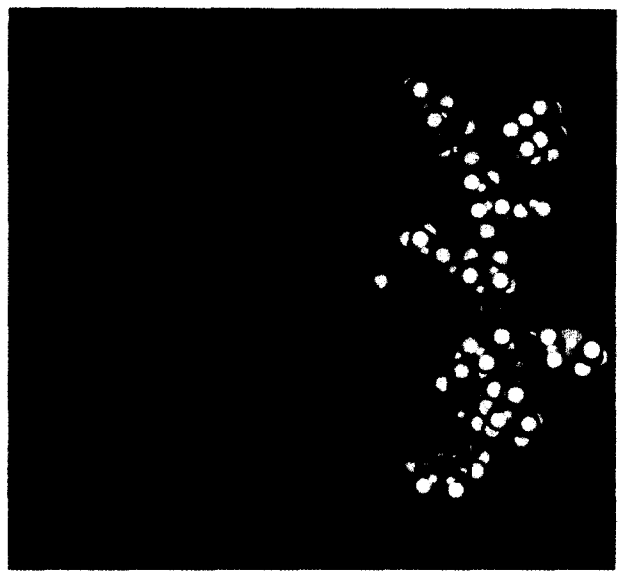

(b)

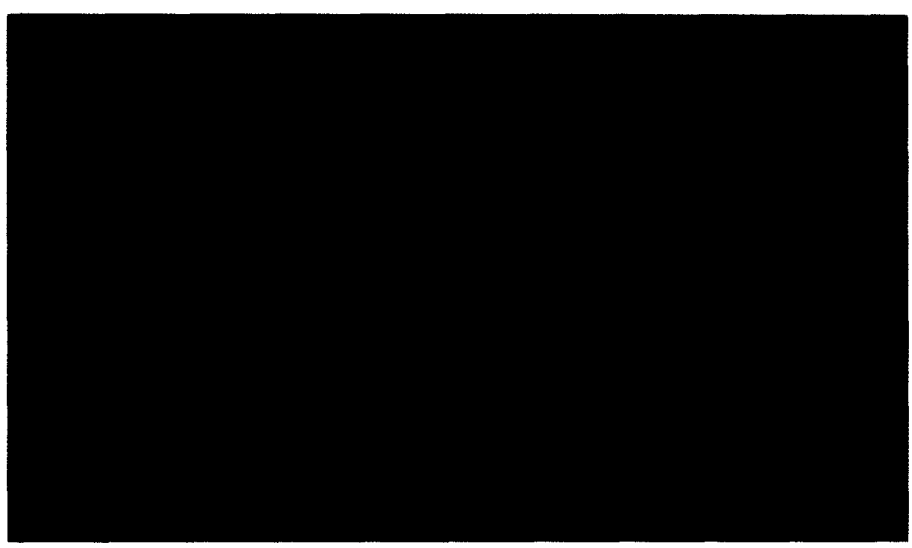

Figure 3. (a) Side view of DARPP-32, residues 31–39, bound to the active site of PP1. DARPP is represented in CPK mode and color coded by atom type: carbon, gray; nitrogen, blue; oxygen, red; sulfur, yellow; hydrogen, white. PP1 is in blue. Metal ions are shown as spheres in fuchsia. (b) Stereo view of DARPP-32, residues 31–39, with the active site contacting residues of PP1. DARPP is color coded by atom type as for (a). PP1 residues are represented in gold. The metal ions are shown as spheres in fuchsia.

tion, and so that the acidic groove residues which may contact DARPP would be included) were allowed to minimize freely while the rest of the protein was held fixed. Minimization and dynamics optimizations were performed as for phosphothreonine. The lowest energy structure is shown in Figure 3. The starting conformation of DARPP docked without restraints gave a set of final structures much higher in energy than those obtained from the restrained molecules. It is interesting to note that out model supports the observation implied in SAR studies[20] (Table 1) that Arg221 is not as critical for binding DARPP as it is for binding calyculin or okadaic acid. Perhaps the arginine contacts an amide carbonyl as is the case for microcystin, but does not form the kind of suggestive specific interaction which we see in our models with calyculin and okadaic acid.

A similar approach was taken for the development of a model structure of PP1 with calyculin. We obtained the initial structure of calyculin A from the Cambridge Structural Database.[17] Calyculin consists of a hydrophobic tail; a phosphate group; a spiroketal moiety; and a basic, peptidomimetic segment. We believe that the spiroketal moiety may, in this case, be imitating the proline turn adjacent to the phosphothreonine residue in DARPP. This type of arrangement allows the molecule to achieve a twist such that the hydrophobic tail fits nicely in the hydrophobic groove. The X-ray structure of calyculin was subjected to a conformational search in which the hydrophobic segment was aligned with the Adda side-chain of microcystin from the X-ray of bound microcystin, and a search in which it was aligned with the model conformation of residues 36–39

of DARPP bound with PP1. In the first orientation, the C15-methoxy of calyculin was overlaid with the C2-methyl of Adda; the C8-methyl of calyculin was overlaid with the C6-methyl of Adda; the C7-methyl of calyculin was overlaid with the C8-methyl of Adda; and, the C2–C3 and C4–C5 double bonds of calyculin were overlaid with the phenyl ring of Adda. In the second orientation, the phosphate of calyculin was superimposed with the phosphate of DARPP; C18 of calyculin was overlaid with the methyl group of the phosphothreonine in DARPP; C16 of calyculin was overlaid with the α-carbon of the phosphothreonine residue of DARPP; the C6–C7 alkene of calyculin was overlaid with the Met-Leu amide bond of DARPP; C5 of calyculin was overlaid with the α-carbon of Leu in DARPP; the C32-amide nitrogen of calculin was overlaid with a terminal nitrogen of Arg31 of DARPP, and the C36-dimethyl-amine nitrogen was overlaid with the other terminal nitrogen of Arg31. These structures were subjected to minimization and dynamics simulations as previously described for the preliminary model structures of DARPP.

In the X-ray structure, calyculin adopts a pseudo-cyclic conformation in which the phosphate group forms hydrogen bonds with the oxazole amine and the C33-amide nitrogen of the peptidomimetic segment. However, to be consistent with our model of DARPP with PP1, the peptidomimetic segment of calyculin was docked in an extended conformation, instead of the cyclic conformation observed in the X-ray, so that the basic oxazole and amide groups reach into the acidic pocket (restrained to 2.90 Å from contacting residues Asp208 and Glu256), and the phosphate oxygens are available for metal-coordination. Distance restraints were set for the phosphate group of calyculin with PP1 based on the model of phosphothreonine with PP1 and the hydrophobic tail of calyculin with PP1 based on the X-ray of Adda with PP1. In addition to four starting conformations docked with PP1 and restrained under the above guidelines, a fifth structure of calyculin was docked with PP1 without distance restraints. As in the prior model structures, subsets were defined 7 Å around the starting conformations of calyculin to encompass the contacting residues of PP1, and the rest of the protein was fixed for minimization and dynamics calculations. The lowest energy structure is exhibited in Figure 4. The structure of calyculin docked without restraints yielded final models with unfavorable steric interactions which were higher in energy than those for which restraints had been imposed. Major potential hydrogen bond contacts are the dimethylamine of calyculin with Glu256 of PP1; the oxazole nitrogen with Asp208 (which is implicated in binding from SAR data, Table 1);[20] the C34 and C35 hydroxyl groups with Asp210 andAsp212, respectively; and, the C11 and C13 hydroxyl groups with Arg221. The latter contacts support the SAR evidence which shows that formation of the acetonide at C11 and C13 results in decreased activity.[3]

Calculation of the Structures of Cantharidic Acid, Okadaic Acid, and Tautomycin with PP1

Models for the phosphatase inhibitors containing a carboxylic acid functionality were to conform to two criteria. The first requirement is that one carboxylate must mimic the phosphate bridging the metal ions. Evidence for this hypothesis is as follows: first, the X-ray structure of microcystin shows that only one of the carboxylates is coordinated to the metals and the other forms a salt bridge with Arg96; second, there is evidence in the literature for coordination of one carboxylate to a bimetallic site;[21] third, the structure of okadaic acid contains only one carboxylate. With this idea for the carboxylate binding mode in mind, the second technique was to model cantharidic acid using the low-energy structure of phosphothreonine as a standard. Several possible orientations of cantharidic acid were modeled such that one carboxylate and adjacent methyl substituent were situated in approximately the same fashion as the metal-complexing phosphate oxygens and the methyl group of phosphothreonine in the model structure. (The orientation of the carboxylate is also consistent with Carrell's observation that a carboxylate binding to a bimetallic center containing manganese does so through the syn lone pairs of the oxygens.)[21] Subsets were defined 7 Å around cantharidic acid for each of the structures and these were subjected to minimization and dynamics calculations. The lowest energy conformation found is shown in Figure 5. The bridging ether oxygen of cantharidic acid appears to contact Tyr272 in our lowest energy structure, and SAR studies[20] show that this ether oxygen is important to binding in the active site. In addition, the non-coordinating carboxylate forms a salt bridge with Arg96 and a contact with Tyr134 which correspond to the contacts made by the non-bridging carboxylate in the X-ray structure of microcystin with PP1.

Docking of the other carboxylate-containing inhibitors was accomplished using this model of cantharidic acid with PP1 as a foundation. Since a significant amount of

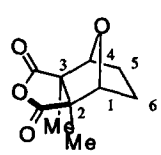

Cantharidin
(insects)

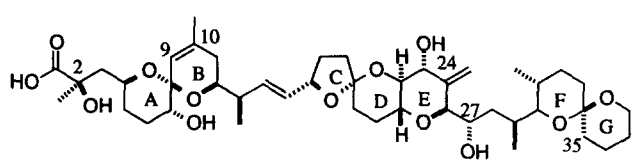

Okadaic acid
(dinoflagellates)

(a)

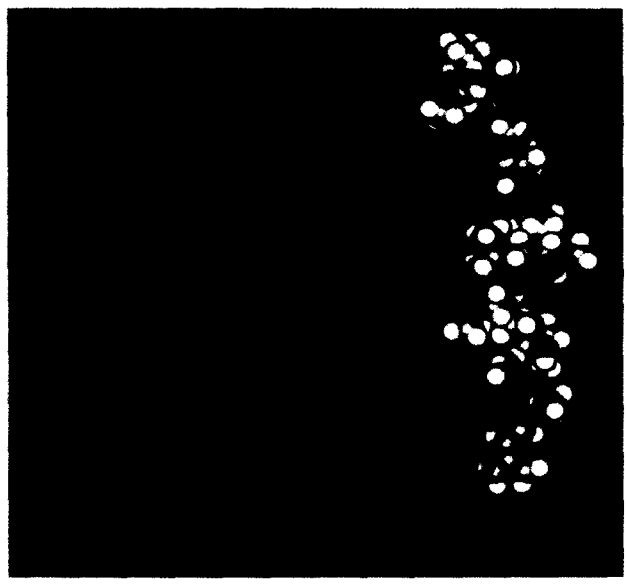

(b)

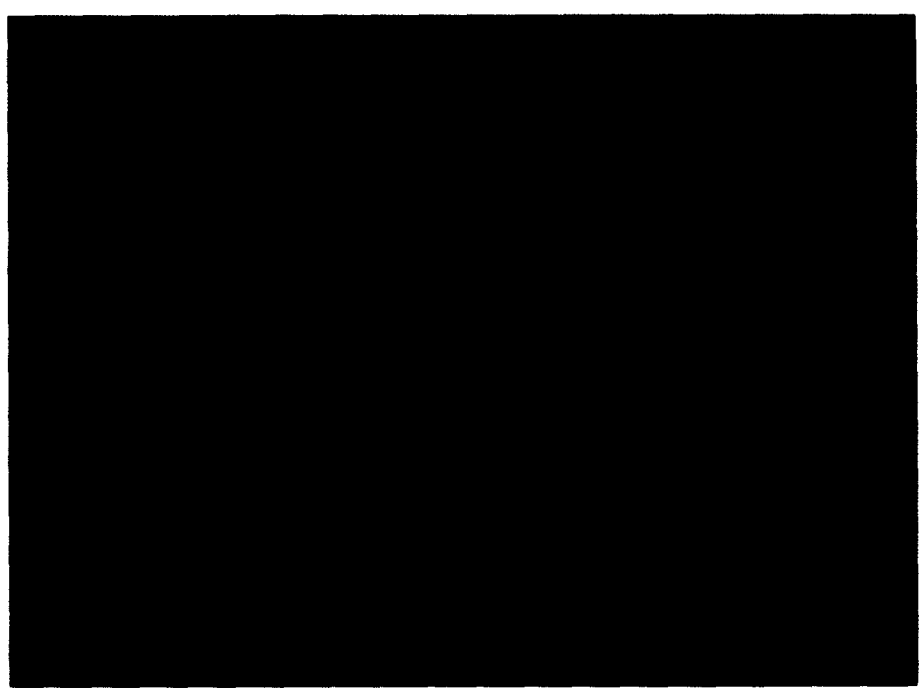

Figure 4. (a) Side view of calyculin bound to the active site of PP1. Calyculin is represented in CPK mode and color coded by atom type: carbon, gray; nitrogen, blue; oxygen, red; hydrogen, white. PP1 is in blue. Metal ions are shown as spheres in fuchsia. (b) Stereo view of calyculin with the active site contacting residues of PP1. Calyculin is color coded by atom type as for (a). PP1 residues are represented in gold. The metal ions are shown as spheres in fuchsia.

the published SAR work has concentrated on okadaic acid, this inhibitor is the next logical choice for modeling studies. Okadaic acid is also a fairly rigid molecule and should have fewer conformational states accessible than the more flexible tautomycin. Mutagenesis studies suggest that the β12–β13 loop of the phosphatases is critical for inhibition by okadaic acid, and this region has been implicated in the observation that okadaic acid is slightly more selective for PP2A than for PP1.[20,22] Therefore, the model structures should show favorable contacts with this region, and a comparison of these complexes should supply a possible explanation. Okadaic acid differs somewhat from microcystin, cantharidic acid, and tautomycin in that it only contains one carboxylate; however, the C2-OH is found to be crucial for activity and could be forming an important hydrogen bond with Arg96 instead of the salt bridge that exists between this residue and the second carboxylate present in the other inhibitors. Other functions for this group may be that it mimics the phosphate ester and is protonated by the general acid His125, or that it contacts Tyr272.

(a)

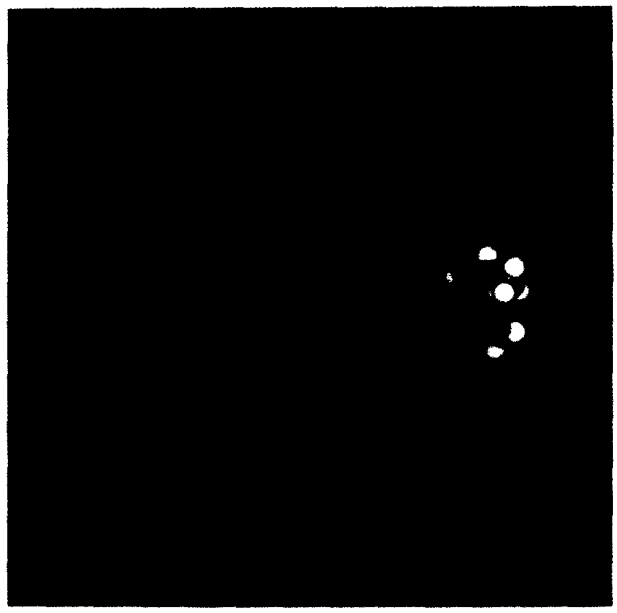

(b)

Figure 5. (a) Side view of cantharidic acid bound to the active site of PP1. Cantharidic acid is represented in CPK mode and color coded by atom type: carbon, gray; nitrogen, blue; oxygen, red; hydrogen, white. PP1 is in blue. Metal ions are shown as spheres in fuchsia. (b) Stereo view of cantharidic acid with the active site contacting residues of PP1. Cantharidic acid is color coded by atom type as for (a). PP1 residues are represented in gold. The metal ions are shown as spheres in fuchsia.

The X-ray structure of okadaic acid was obtained from the Cambridge Structural Database.[9,10] To arrive at a model structure suitable for docking with PP1, we superimposed the carboxylate of okadaic acid with the C3-carboxylate of the cantharidic acid model, the C2-methyl of okadaic acid with the C3-methyl of cantharidic acid, the C2–C3 bond of okadaic acid with the C3–C4 bond of cantharidic acid, and the C2-alcohol of okadaic acid with the C2-carboxylate of cantharidic acid. This structure was minimized following the standard protocol (see Materials and Methods). Next, the five lowest energy conformers of okadaic acid were docked with PP1. Distance restraints for four of the starting structures were set based on the model of cantharidic acid with PP1. Additional restraints (within 3 Å) were set between the A and B rings of okadaic acid and the β12–β13 loop; and the E, F, and G rings with key residues in the hydrophobic pocket. Subsets were

(a)

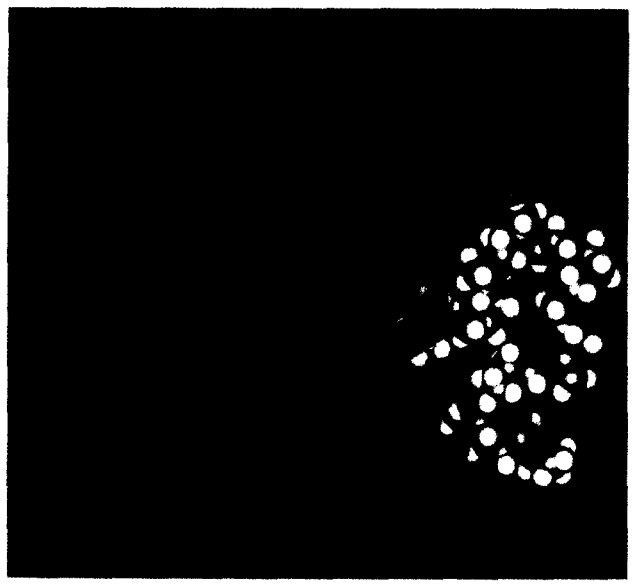

(b)

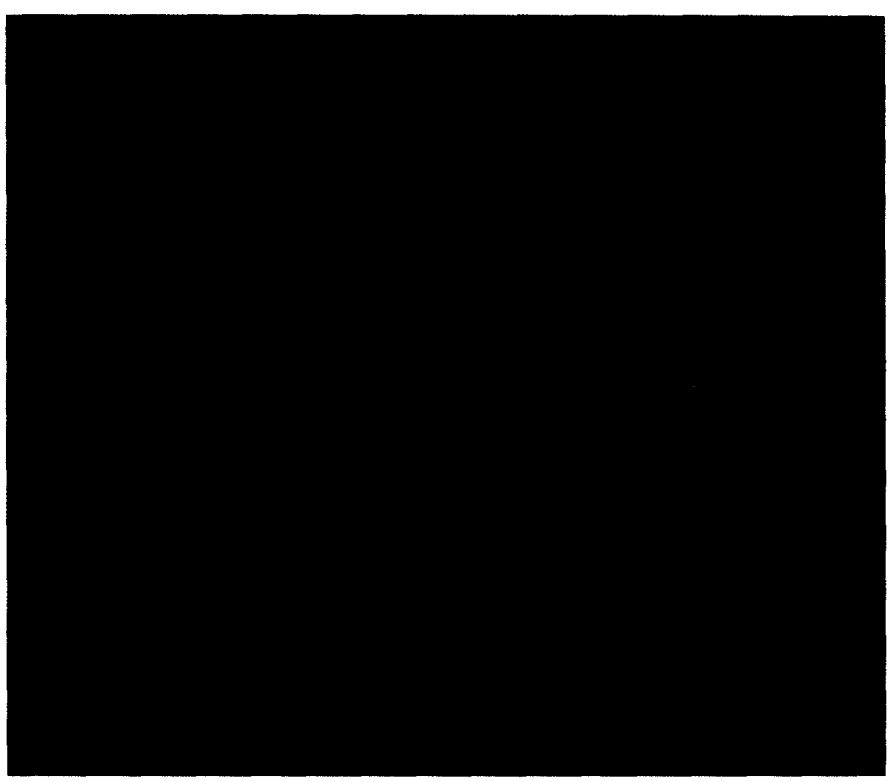

Figure 6. (a) Side view of okadaic acid bound to the active site of PP1. Okadaic acid is represented in CPK mode and color coded by atom type: carbon, gray; nitrogen, blue; oxygen, red; hydrogen, white. PP1 is in blue. Metal ions are shown as spheres in fuchsia. (b) Stereo view of okadaic acid with the active site contacting residues of PP1. Okadaic acid is color coded by atom type as for (a). PP1 residues are represented in gold. The metal ions are shown as spheres in fuchsia.

defined 8 Å around okadaic acid to include all potentially contacting residues. Docking of either the X-ray structure of okadaic acid or a minimized structure without restraints provided final structures which were higher in energy than the final structures from docked molecules with restraints, or had unfavorable steric overlaps. The most energetically favorable structure found is depicted in Figure 6. Inspection of this model structure shows a potential hydrogen bond between the

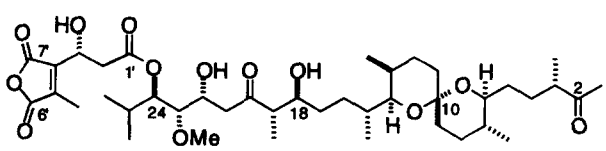

Tautomycin
(*Streptomyces* bacterium)

C24-OH, the C27-OH, and Arg221. Several important hydrophobic interactions with the β12–β13 loop may also be inferred from this model; the methyl group of okadaic acid at C10 contacts Tyr272 and the methyl at C13 contacts Phe276. In addition, the methyl group at C29 appears to contact Tyr134.

Perhaps the most difficult model to propose is that for tautomycin with PP1. Tautomycin has many conformational degrees of freedom and can therefore access more favorable states than the other inhibitors. An additional disadvantage is that there are few SAR studies published for tautomycin with the phosphatases. In this case, our strategy must be to generate a structure based on the common structural motifs between tautomycin and okadaic acid which shows interactions that we believe may be important for recognition; and then, to optimize this structure to find a low energy state. We assume that the anhydride of tautomycin is hydrolyzed to the diacid in vivo, and that it is the diacid which serves as the phosphate mimic.[5] Incorporating this idea in our model, the C6′-carboxylate of tautomycin was superimposed with the C3-carboxylate of cantharidic acid, the C5′-methyl was superimposed with the C3-methyl of cantharidic acid, and the C7′-carboxylate of tautomycin was superimposed with the C2-carboxylate of cantharidic acid. Additional overlays included the C25-methyl of tautomycin and the C10-methyl of the bound okadaic acid model, the C23-methoxy of tautomycin with the C7-OH of okadaic acid, the C3-methyl of tautomycin with the C31-methyl of okadaic acid, the C7-methyl of tautomycin with the C29-methyl of okadaic acid, and the B-ring of tautomycin with the E-ring of okadaic acid. Five starting geometries fitting the described criteria were subjected to minimization and dynamics.

For the models of tautomycin bound with PP1, we docked and restrained the C6′-carboxylate such that it coordinates to the metal ions as does the C3-carboxylate in the cantharidic acid model; and the C7′-carboxylate was restrained to Arg96 like the C2-carboxylate in the cantharidic acid model. The C3′-OH may function as the phosphate ester mimic and contact His125 and/or Tyr272, and was restrained accordingly. Like okadaic acid, tautomycin may bind to the β12–β13 loop of the phosphatases; distance restraints (approximately 3 Å) were set from C18–C22 of tautomycin to potentially contacting residues in the β12–β13 loop. In addition, the spiroketal segment of tautomycin was docked and restrained (also approximately 3Å) to key residues in the hydrophobic pocket. Subsets were defined 11.0 Å around tautomycin. As per previous simulations, four distinct structures conforming to the above guidelines were minimized, and one in which no restraints were imposed was minimized. The lowest energy final structure (not resulting from the unrestrained model) is shown in Figure 7. Several interesting contacts are discernible from this model; namely, the C25-methyl of tautomycin and Tyr272, the C19-methyl and Phe276, the C18-OH and Glu275, the C7-methyl and Tyr134, and the C3-methyl and Trp206. Another attractive feature is the potential contact between Arg221 and both the ester carbonyl at C1′ and the C22-OH, which has been shown to be critical for inhibiton;[5] this is very similar to the key amide carbonyl–Arg221 interaction observed in the X-ray structure of microcystin with PP1.

Calculation of the Structure of Microcystin–PP2A Complex and the Structures of the OA Class Inhibitors with PP2A

The first step in the development of binding models is to predict the structure of PP2A based on its ~50% homology with the known structure of PP1. The PP2A model structure was created on a Silicon Graphics workstation using the Homology 2.3 module in the Insight *II* 2.3.7 graphic molecular modeling program developed by Biosym Technologies Inc. The model PP2A structure was based on X-ray structural coordinates of the homologous protein PP1.[18] Following the homology protocol, the X-ray structure of PP1 was initially refined by minimization in the Discover 2.9.5 module. At this stage, the metal ions of PP1 had to be excised in order to extract the peptide sequence in homology. Next, the sequences of PP1 and PP2A were aligned according to their homologous regions (Fig. 8). Structurally conserved regions (SCR) were then defined for PP2A based on the known secondary structures in PP1. Nonstructurally conserved regions were defined as designated loops, in which the coordinates for variable regions are appropriated corresponding to those for the respective residues in the reference protein. In order to relieve any unfavorable sidechain overlaps and nonbond energies introduced in the model structure, the Measure/Bump and Residue/Auto_Rotamer commands were applied. Finally, the model structure was optimized in the Discover 2.9.5 module by minimizing over 10,000 steps until convergence was reached at a maximum derivative of 0.001 kcal/mol Å.

The preliminary conformation of microcystin for docking with PP2A was obtained directly from the X-ray structure of microcystin LR bound to PP1.[19] Microcystin interacts with PP1 in a Y-shaped groove on the protein surface at three sites: an active site metal, the proximal hydrophobic binding cleft, and a peptide-binding groove that extends towards the *C*-terminus. Specifically, the isoglutamic acid carboxylate that is crucial for inhibition by microcystin is hydrogen-bonded to both Tyr272, and a water ligand that coordinates the Fe atom. Cys273, found in the β12–β13 loop, has conjugately added to the dehydroalanine of microcystin. The other carboxylate of microcystin is H-bonded to Arg96 and Tyr134, and the other conserved Arg221 interacts with the carbonyl of Adda. The conformation of the macrocycle is in a figure of eight—dramatically different to the calculated structure of Quinn and coworkers, but quite similar to the solution conformation of microcystin determined by Bagu.[23] Finally, Adda snugly fits into the hydrophobic binding cleft.

(a)

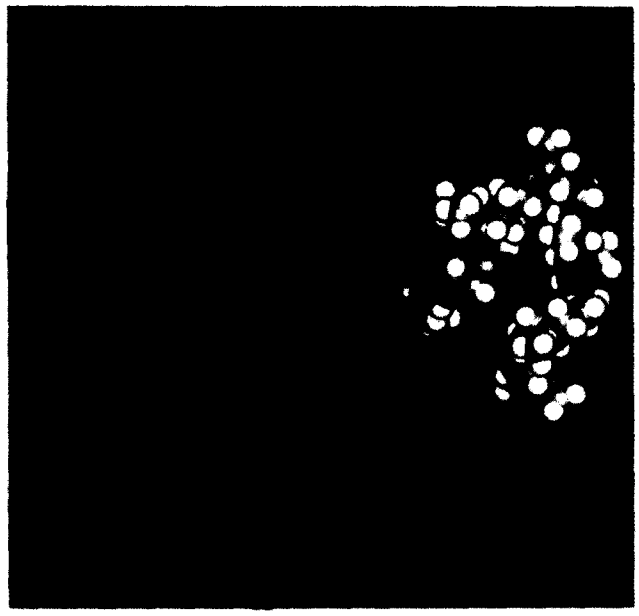

(b)

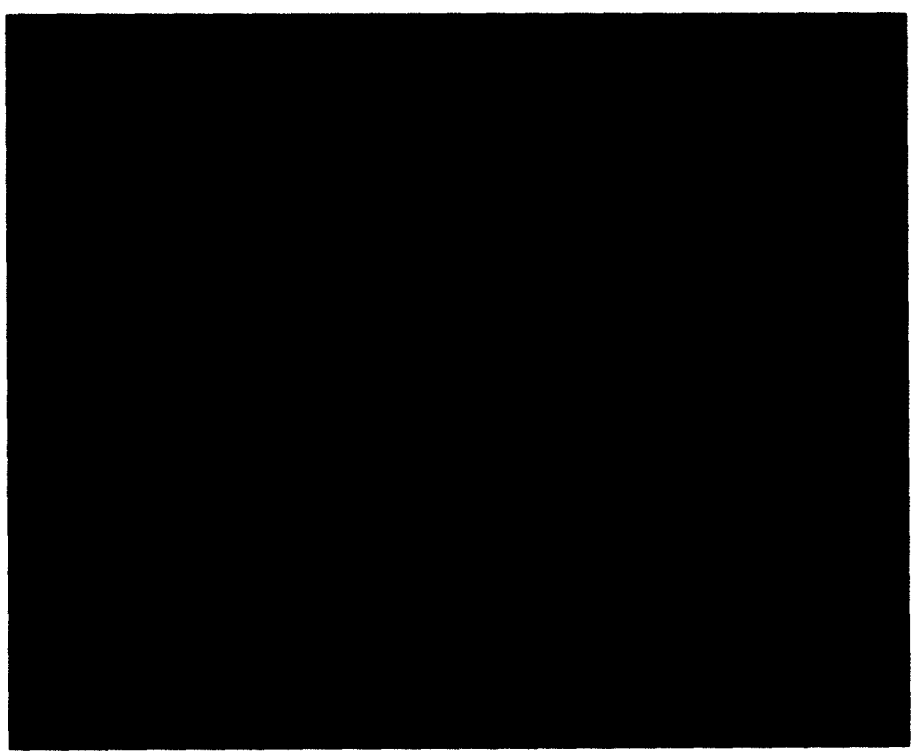

Figure 7. (a) Side view of tautomycin bound to the active site of PP1. Tautomycin is represented in CPK mode and color coded by atom type: carbon, gray; nitrogen, blue; oxygen, red; hydrogen, white. PP1 is in blue. Metal ions are shown as spheres in fuchsia. (b) Stereo view of tautomycin with the active site contacting residues of PP1. Tautomycin is color coded by atom type as for (a). PP1 residues are represented in gold. The metal ions are shown as spheres in fuchsia.

The inhibitor was manually docked into the PP2A binding site by positioning the *N*-methyl-dehydroalanine residue of microcystin at a distance of 1.72 Å from Cys 273 (C–S distance) to which it is presumed to be covalently bound, and by preserving all of the major contacts observed between microcystin and PP1; that is, no more than a 0.5 Å deviation from the respective distances in the crystal structure was allowed. At this point, it was presumed that a reasonable initial guess had been achieved. Minimization and dynamics calculations were performed using the Discover_3 (version 3.0) module. Subsets were defined for the active site of PP2A, which included residues at a distance of 12 Å surrounding microcystin, and the nonactive site, which corresponded to the rest of the protein not participating in binding. The nonactive site was held fixed during the

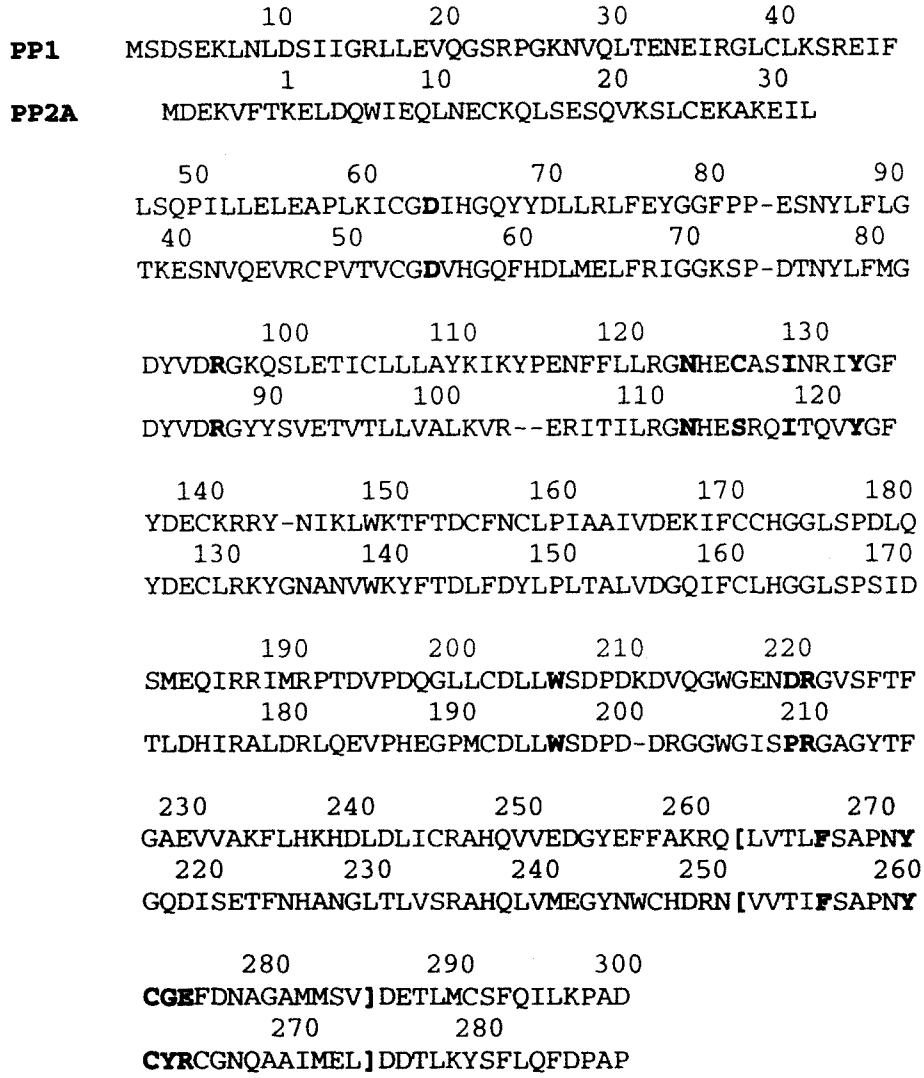

Figure 8. Sequence comparison of PP1 and PP2A. Residues highlighted in blue are conserved and contact microcystin in both PP1 and the model of PP2A. Residues highlighted in magenta are those that contact microcystin in both proteins, but are not conserved and could be exploited for microcystin analogue development. Residues contained within red brackets belong to the β12–β13 loop, which is thought to play an important role in inhibitor recognition.

calculations, and distance constraints were imposed on the carboxylate groups of microcystin: they were restrained to a 3 Å variance from the contacting residues in the proposed phosphate binding site. Convergence after minimization was reached at 20,000 steps and 0.01 kcal/mol Å. Dynamics simulations were performed on this structure, and the resultant lowest energy model is shown in Figure 9. All subsequent calculations for PP2A and the other inhibitors were performed following the same protocol including the same number of iterations and the same convergence limit.

Guided by the preceding model of PP1-DARPP, a model of DARPP with PP2A was generated. Once again, the *N*-terminal arginine residues of DARPP were tethered to residues in the 'acidic groove', which for PP2A are Glu242, Asp200, and Asp201. Interestingly, the region of PP2A corresponding to the 'acidic groove' is not entirely homologous to PP1; it contains fewer acidic moieties, and these do not coincide precisely with those for PP1. The rest of the DARPP-PP2A model was docked in the same fashion as it was for DARPP-PP1. Subsets were defined for the region 11 Å around DARPP. Minimization and dynamics calculations afforded the low energy structure shown in Figure 10.

A preliminary docking model was created for calyculin with PP2A by analogy with the calculated structure of PP1-calyculin. Calculations were carried out as before with a subset 8 Å around calyculin permitted to relax, and the lowest energy structure is shown in Figure 11. Major contacts in this model structure include the dimethylamine of calyculin with Glu242 of PP2A; the oxazole nitrogen with Asp198; the C34 and C35 hydroxyl groups with Asp200 and Asp201; and the C11 and C13 hydroxyl groups with Arg210. Furthermore, as is noted in the SAR data provided in Table 1,[20]

(a)

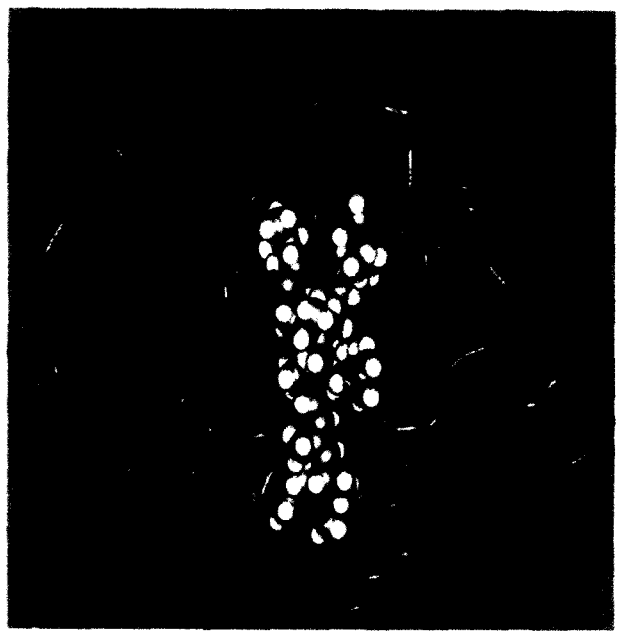

(b)

Figure 9. (a) Front view of microcystin bound to the active site of PP2A. Microcystin is represented in CPK mode and color coded by atom type: carbon, gray; nitrogen, blue; oxygen, red; hydrogen, white. PP2A is in pink. Metal ions are shown as spheres in fuchsia. (b) Stereo view of microcystin with the active site contacting residues of PP2A. Microcystin is color coded by atom type as for (a). PP2A residues are represented in gold. The metal ions are shown as spheres in fuchsia.

substitution of Cys127 in PP1 to serine (which is present at the same site in PP2A, Ser116), affects binding of calyculin. There may be a contact between the terminal cyano group of calyculin and this side-chain.

A model was generated for cantharidic acid with PP2A showing essentially the same contacts as for PP1–cantharidic acid. There was one possible exception which may have some effect on the selectivity of cantharidin for PP2A: Tyr263 may also contact the bridging ether. This structure is given in Figure 12.

A slightly different initial starting geometry was chosen for okadaic acid with PP2A than for PP1 with okadaic

(a)

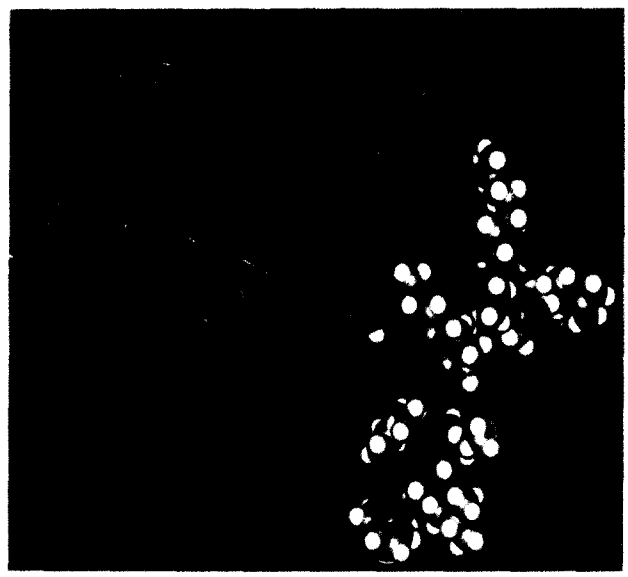

(b)

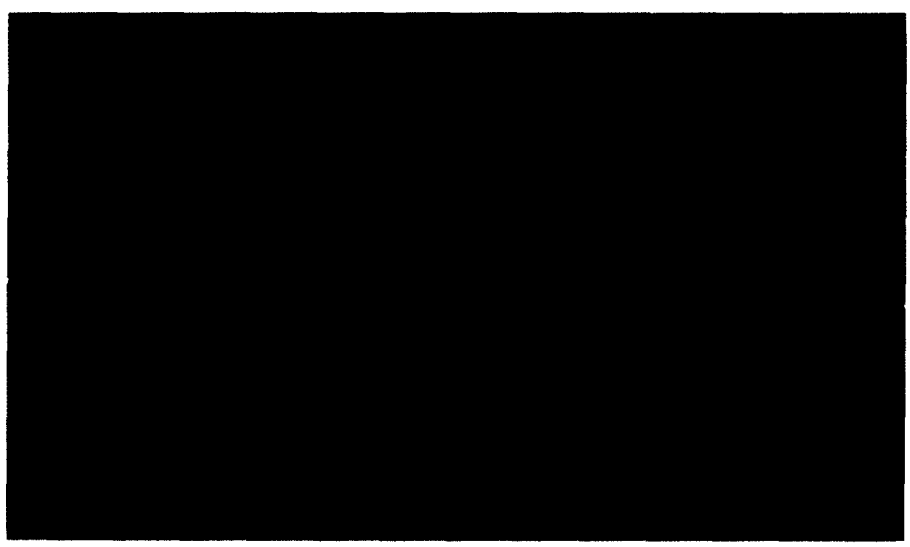

Figure 10. (a) Side view of DARPP-32, residues 31–39, bound to the active site of PP2A. DARPP is represented in CPK mode and color coded by atom type: carbon, gray; nitrogen, blue; oxygen, red; sulfur, yellow; hydrogen, white. PP2A is in pink. Metal ions are shown as spheres in fuchsia. (b) Stereo view of DARPP-32, residues 31–39, with the active site contacting residues of PP2A. DARPP is color coded by atom type: carbon, gray; nitrogen, blue; oxygen, red; hydrogen, white. PP2A residues are represented in gold. The metal ions are shown as spheres in fuchsia.

acid. As can be seen from a comparison of the amino acid sequences of the two phosphatases in the critical β12–β13 loop, PP2A has two potentially significant residues which differ from PP1. Therefore, the model structure of okadaic acid with PP2A should show contacts with these residues. Excepting these contacts, the rest of the interactions believed to play a role between okadaic acid and PP1 were preserved. Subsets were defined 9 Å around okadaic acid and were permitted to minimize freely before dynamics simulations. The lowest energy structure is provided in Figure 13. Examination of the β12–β13 region of this model structure shows that there are potential contacts between the C10-methyl of okadaic acid and Tyr263 of PP2A (as opposed to Tyr261 which is corresponds to Tyr272 in PP1) and the C7-OH and Arg264 (which corresponds to Glu275 in PP1). The latter contact may account for the selectivity observed with PP2A in this region. Other possible contacts which relate to those found with PP1 are the C24-OH and C27-OH with Arg210, and the C29-Me with Tyr123.

As for okadaic acid, a slightly different docking model than that with PP1 was constructed for tautomycin with PP2A to accommodate the changes in the β12–β13 loop. The carboxylates were positioned as for tautomycin with PP1. Subsets were defined 10 Å around tautomycin for minimization and dynamics calculations. The final optimized structure is shown in Figure 14. Key interactions are those between: the C25-methyl groups of tautomycin and Tyr261 and Tyr263 of PP2A, the C22-OH and Arg264 (which corresponds to Glu275 in PP1), the C7-methyl and Tyr123, and the C3-methyl

Table 2. A summary of the contacts between the OA class inhibitors and the catalytic site residues of PP1 and PP2A

Inhibitor/contacting group	PP1 residue(s)	PP2A residue(s)
Cantharidic acid		
8-O (bridging)	Tyr272	Tyr261, *Tyr263*
C3-COO–	Arg96	Arg87
C3-COO–	Tyr134	Tyr123
C2-Me	His248	His237
Okadaic acid		
C24-OH	Arg221	Arg210
C27-OH	Arg221	Arg210
C10-Me	Tyr272	*Tyr263*
C13-Me	**Phe276**	—
C29-Me	Tyr134	Tyr123
C2-OH	Arg96	Arg87
C7-OH	—	*Arg264*
C2-Me	His248	His237
Tautomycin		
C25-Me	Tyr272	Tyr261, *Tyr263*
C19-Me	**Phe276**	—
C18-OH	**Glu275**	—
C7-Me	Tyr134	Tyr123
C3-Me	Trp206	Trp196
C1′(O)	Arg221	Arg210
C22-OH	Arg221	*Arg264*
Calyculin		
C36-NMe2	Glu256	*Glu242*
C27-N	Asp208	Asp198
C34-OH	Asp210	Asp200
C35-OH	Asp212	*Asp201*
C11-OH, C13-OH	Arg221	Arg210
DARPP-32		
Arg38	**Glu252**, Glu256	*Glu242*
Arg39	Asp210, Asp212	Asp200, *Asp201*

Differential points of contact are highlighted in **boldface** type for PP1 and *italic* type for PP2A; highlighted residues are those which are either nonconserved or do not correspond to the same residues in both proteins (see Fig. 8).

and Trp196. Like the PP1-tautomycin model, there is a contact between the C24-ester carbonyl and Arg210.

A comparison of the proposed contacts between the OA class inhibitors and the corresponding residues in PP1 versus PP2A is provided in Table 2. For sequence correlation between the two proteins, please refer to Figure 8.

Comparision of the Model Bound Conformations

Inspection of the model bound conformations of the inhibitors reveals the anticipated conformity in the relative alignment of the putative phosphothreonine mimics (Fig. 15). This result is consistent with our prediction that the inhibitors all bind through the similar orientation of a common pharmacophore. As expected, there are some discrepancies between our structures, the X-ray structures of the unbound inhibitors, and models of the unbound inhibitors which ostensibly reached global minima. Superficially, however, all of the structures except calyculin and cantharidin appear to form a macrocycle which could achieve the major contacts in the phosphate binding site, and a hydrophobic tail to fit into the hydrophobic groove.

The crystal structure of free okadaic acid shows that the molecule arches back on itself as it does in our model perhaps to form a hydrogen bond between the carboxylate and the C24-OH.[9,10] Formation of this arch exposes the C10-methyl and the C13-methyl of okadaic acid to the surface in the X-ray structure and propitiously, to the β12–β13 loop in our models. In order to achieve this interaction, however, the carboxylate must be in a different rotamer than in our model. A second contrast between the X-ray structure and the model is that the C27-OH and the C24-OH in the model both interact with Arg221 of PP1 (Arg210 of PP2A); therefore, the rotamer at C27 is different in the model than in the X-ray so that this contact may be made.

Visual analysis of the X-ray structure of calyculin shows one notable incongruity with the model structure: the peptidomimetic segment folds over so that the phosphate group may form potential hydrogen bonds with the oxazole amine and the C33 amide nitrogen.[17] In the model, the peptidomimetic segment occupies the 'acidic groove' binding site of the protein. However, the hydrophobic tail of calyculin is in a strikingly similar conformation in the X-ray structure as in the model. Both hydroxyl groups (at C11 and C13) are together in

(a)

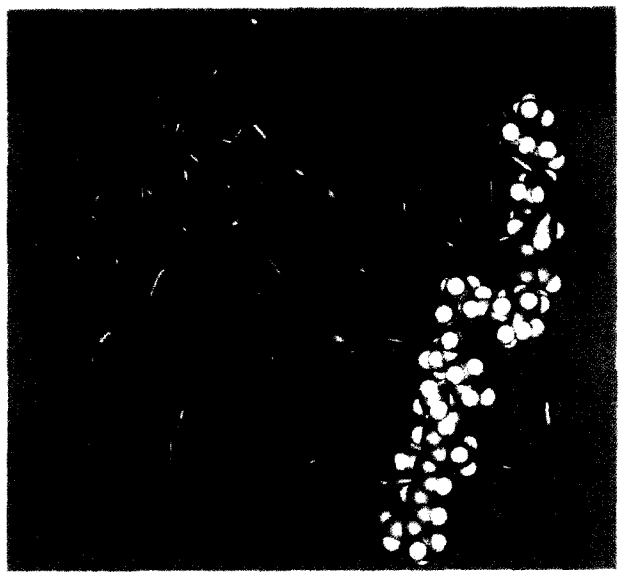

(b)

Figure 11. (a) Side view of calyculin bound to the active site of PP2A. Calyculin is represented in CPK mode and color coded by atom type: carbon, gray; nitrogen, blue; oxygen, red; hydrogen, white. PP2A is in pink. Metal ions are shown as spheres in fuchsia. (b) Stereo view of calyculin with the active site contacting residues of PP2A. Calyculin is color coded by atom type: carbon, gray; nitrogen, blue; oxygen, red; hydrogen, white. PP2A residues are represented in gold. The metal ions are shown as spheres in fuchsia.

the same plane in the X-ray and in the model; and the methoxy group at C15 is oriented away from the C13 hydroxyl in both structures. This arrangement of hydroxyl groups is important in our model since we believe that these groups contact Arg221 of PP1 (Arg210 in PP2A).

As discussed earlier, most of the previous model studies relied on conformational searching of plausible preliminary structures based on NOE NMR data and SAR data to arrive at global minima.[24] The results of these studies also contrast with our model bound conformations. Both Quinn's and Murata's[1,14] analyses of okadaic acid afforded structures which were internally hydrogen bonded. Obviously, if the acidic moiety is involved in either metal coordination or in contacting active site residues, it is most likely not going to participate in an internal hydrogen bond. The same argument may be made against Sugiyama et al.'s model of tautomycin[5] in which tautomycin's acidic group and spiroketal segment

(a)

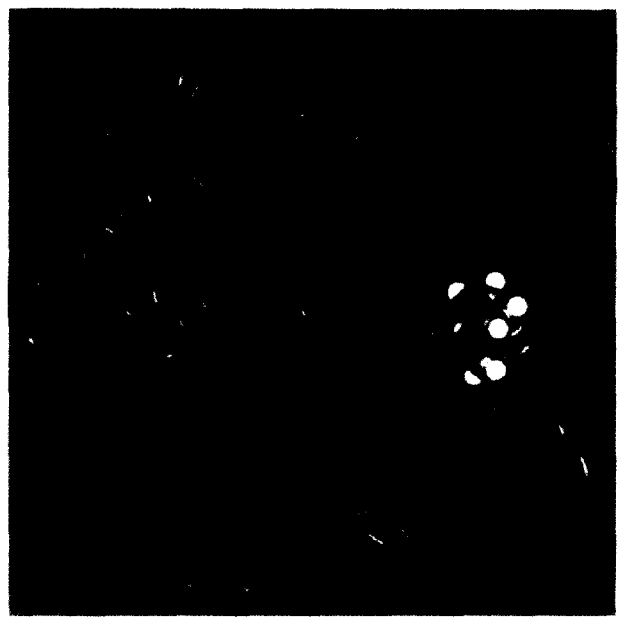

(b)

Figure 12. (a) Side view of cantharidic acid bound to the active site of PP2A. Cantharidic acid is represented in CPK mode and color coded by atom type: carbon, gray; nitrogen, blue; oxygen, red; hydrogen, white. PP2A is in pink. Metal ions are shown as spheres in fuchsia. (b) Stereo view of cantharidic acid with the active site contacting residues of PP2A. Cantharidic acid is color coded by atom type: carbon, gray; nitrogen, blue; oxygen, red; hydrogen, white. PP2A residues are represented in gold. The metal ions are shown as spheres in fuchsia.

were superimposed with those of okadaic acid. However, these structures do bear a general resemblance to our models in their backbone conformation.

The calculated structure of calyculin-A modeled by Quinn et al.[1] forms an internally H-bonded structure similar to that of the X-ray structure. Such a structure would most likely perturb the β12–β13 region, and there are no structure–activity studies to date that would substantiate such an interaction.

The most significant conclusion of the Quinn cyclic peptide modeling study was that the Arg side-chain in microcystin-LR and nodularin is exposed to the surface (i.e., does not interact with either carboxylate) and is not important to binding.[2] This was supported by the X-ray crystal structure and by structure–activity studies undertaken by Fujiki's group.[16] However, the Quinn et al. study also predicted a planar conformation for the peptide rings of microcystin-LR and nodularin. As can be seen by inspection of the X-ray structure of bound

(a)

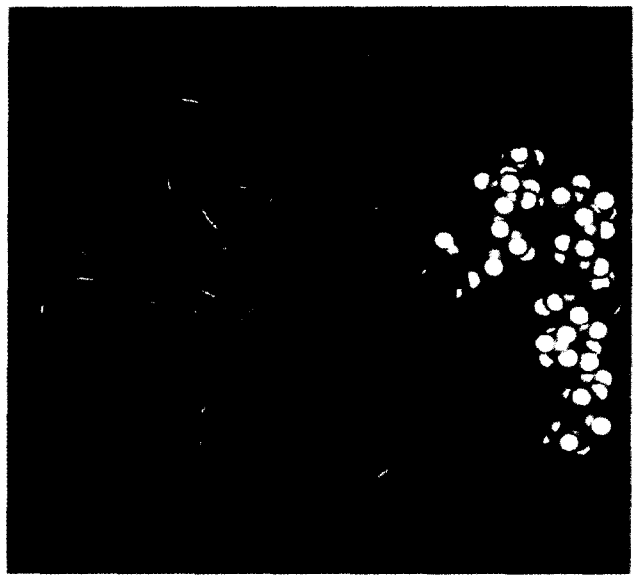

(b)

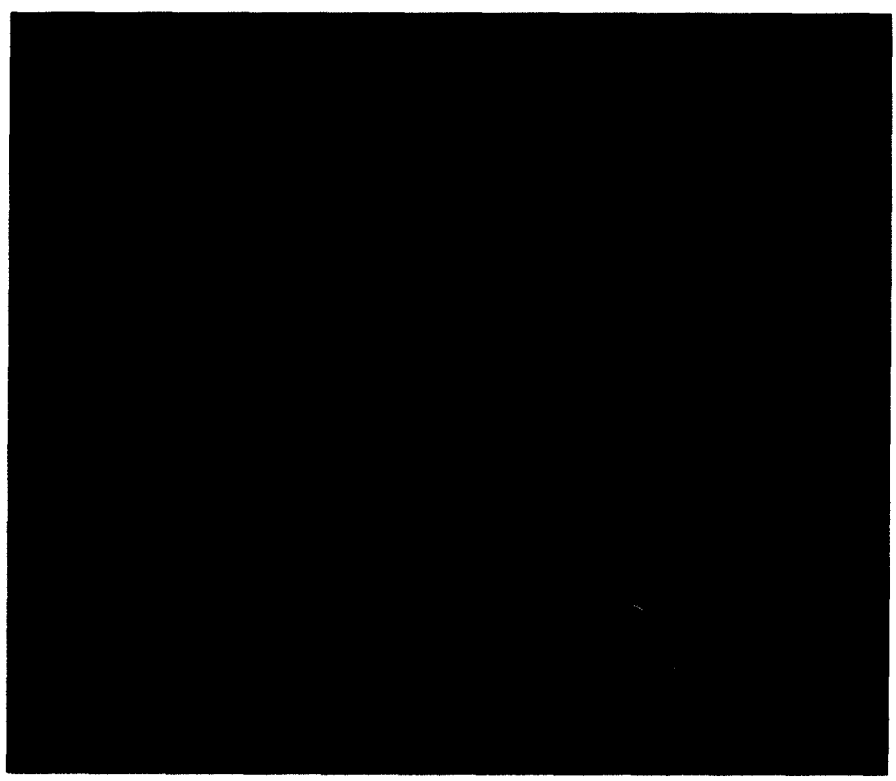

Figure 13. (a) Side view of okadaic acid bound to the active site of PP2A. Okadaic acid is represented in CPK mode and color coded by atom type: carbon, gray; nitrogen, blue; oxygen, red; hydrogen, white. PP2A is in pink. Metal ions are shown as spheres in fuchsia. (b) Stereo view of okadaic acid with the active site contacting residues of PP2A. Okadaic acid is color coded by atom type: carbon, gray; nitrogen, blue; oxygen, red; hydrogen, white. PP2A residues are represented in gold. The metal ions are shown as spheres in fuchsia.

microcystin-LR, the peptide ring is actually twisted in a figure of eight type of conformation to allow critical contacts between the carboxylates and the active site. Perhaps most convincingly, this result demonstrates the limitations of computer modeling studies at predicting bound conformations if the structure of the enzyme active site cannot be taken into account.

Materials and Methods

All models were generated on a Silicon Graphics workstation using the Biopolymer module of the Insight *II* version 95.0 software (released October 1995) developed by Biosym/MSI Technologies Inc. of San Diego. Minimization and dynamics calculations were

(a)

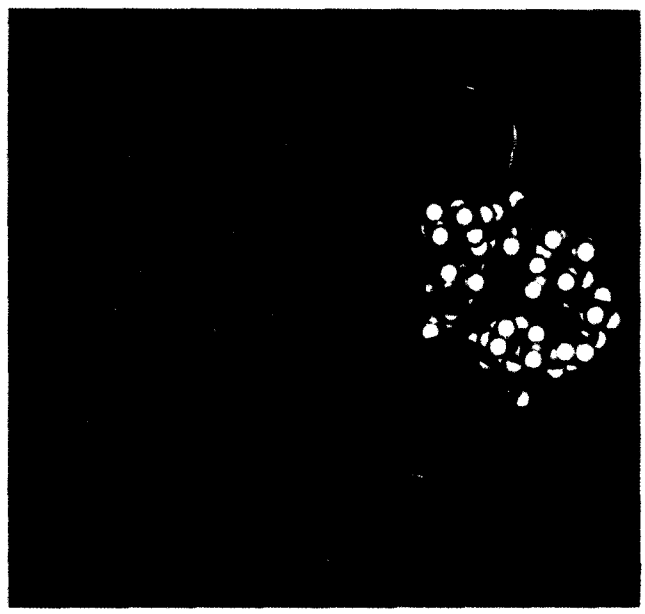

(b)

Figure 14. (a) Side view of tautomycin bound to the active site of PP2A. Tautomycin is represented in CPK mode and color coded by atom type: carbon, gray; nitrogen, blue; oxygen, red; hydrogen, white. PP2A is in pink. Metal ions are shown as spheres in fuchsia. (b) Stereo view of tautomycin with the active site contacting residues of PP2A. Tautomycin is color coded by atom type: carbon, gray; nitrogen, blue; oxygen, red; hydrogen, white. PP2A residues are represented in gold. The metal ions are shown as spheres in fuchsia.

performed using the Discover program (Discover_3 module) with the CFF91 forcefield of Biosym/MSI. Minimizations were performed on five initial starting geometries of each inhibitor bound to both proteins. Dynamics simulations were run at an initial temperature of 300 K over 5000 fs (with a timestep of 1 fs) and at constant volume for each minimized structure, and a total of 100 structures was obtained per simulation. The lowest energy conformers of the dynamics simulations were ultimately resubjected to a final minimization to arrive at the final structures. Dynamics simulations were also attempted at 400 and 600 K under the same conditions as at 300 K in an effort to access lower energy minima. However, the lowest energy structures obtained from the simulation at 400 K were almost identical to those observed at 300 K; and at 600 K, all of the structures were extremely distorted and high in energy.

(a)

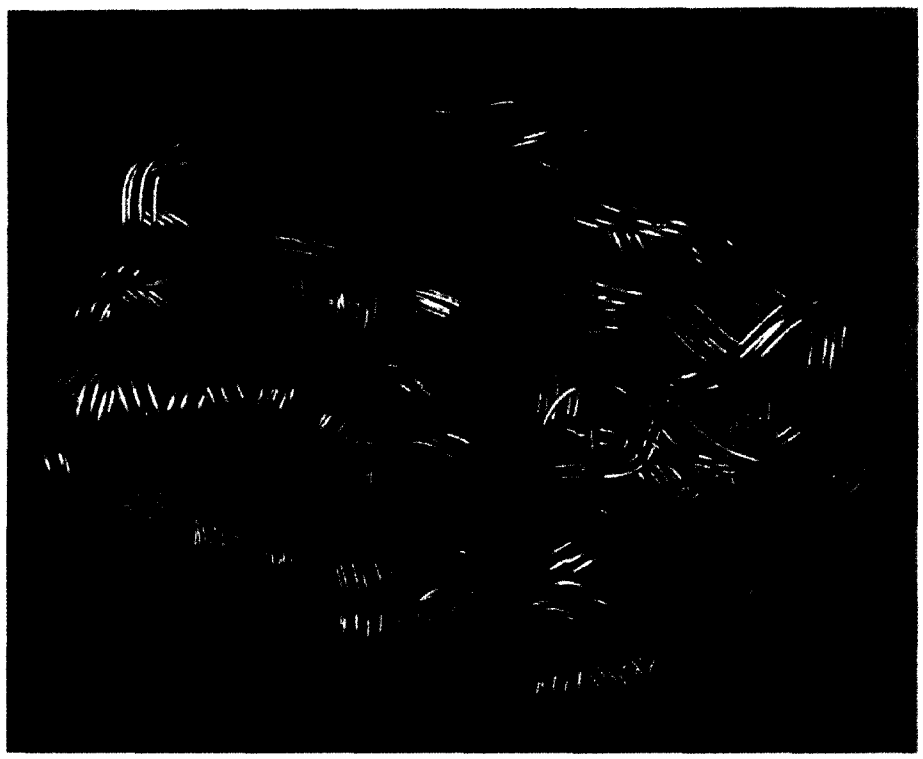

(b)

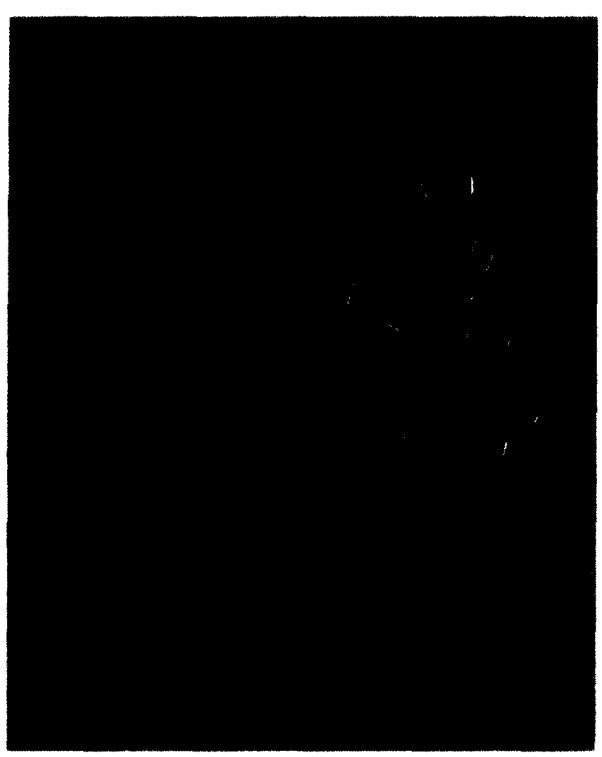

Figure 15. (a) Comparison of the model bound conformations of the inhibitors with PP1: cantharidic acid is shown in orange; calyculin is shown in blue; tautomycin is shown in purple; microcystin is shown in cyan; okadaic acid is shown in pink; all models of PP1 complexed with their respective inhibitors are shown as gray ribbons; metal ions are shown as spheres in fuchsia. (b) Side view of cantharidic acid, calyculin, tautomycin, microcystin, and okadaic acid bound to PP1. Molecules are color-coded as for (a). PP1 is represented in blue ribbon.

Acknowledgements

The authors would like to thank Dr John Kuriyan for providing the X-ray crystal coordinates of the PP1–microcystin-LR complex. We would also like to thank Dr Terry LePage of the UCI Molecular Modeling Facility for her expertise and assistance with the computer software. C.M.G. wishes to acknowledge support by the National Institute on Aging, National Research Service Award AG00096-14 from University of California Irvine.

References

1. Quinn, R. J.; Taylor, C.; Suganuma, M.; Fujiki, H. *Bioorg. Med. Chem. Lett.* **1993**, *3*, 1029.

2. Taylor, C.; Quinn, R. J.; McCulloch, R.; Nishiwaki-Matsushima, R.; Fujiki, H. *Bioorg. Med. Chem. Lett.* **1992**, *2*, 299.

3. Sheppeck, II J. E., Gauss, C.-M., Chamberlin, A.R. *Bioorg. Med. Chem.* **1997**, *5*, 1739.

4. Ubukata, M.; Cheng, X.-C.; Isobe, M.; Isono, K. *J. Chem. Soc. Perkin Trans I* **1993**, 617.

5. Sugiyama, Y.; Ohtani, I. I.; Isobe, M.; Takai, A.; Ubukata, M.; Isono, K. *Bioorg. Med. Chem. Lett.* **1996**, *6*, 3.

6. Hemmings, H. C. J.; Nairn, A. C.; Elliott, J. I.; Greengard, P. *J. Biol. Chem.* **1990**, *265*, 20369.

7. Deana, A. D.; MacGowan, C. H.; Cohen, P.; Marchiori, F.; Meyer, H. E.; Pinna, L. A. *Bioch. Biophys. Acta* **1990**, *1051*, 199.

8. Agostinis, P.; Goris, J.; Waelkens, E.; Pinna, P. A.; Marchiori, F.; Merlevede, W. *J. Biol. Chem.* **1987**, *262*, 1060.

9. Tachibana, K.; Scheuer, P. J.; Tsukitani, Y.; Kikuchi, H.; Van Engen, D.; Clardy, J.; Gopichand, Y.; Schmitz, F. J. *J. Am. Chem. Soc.* **1981**, *103*, 2469.

10. Schimitz, F. J.; Prasad, R. S.; Gopichaud, Y.; Hossain, M. B.; van der Helm, D.; Schmidt, P. *J. Am. Chem. Soc.* **1981**, *103*, 2467.

11. Nishiwaki, S.; Fujiki, H.; Suganuma, M.; Furuya-Suguri, H.; Matsushima, R.; Iida, Y.; Ojika, M.; Yamada, K.; Uemura, D.; Yasumoto, T.; Schmitz, F. J.; Sugimura, T. *Carcinogenesis* **1990**, *11*, 1837.

12. Takai, A.; Murata, M.; Torigoe, K.; Isobe, M.; Mieskes, G.; Yasumoto, T. *Biochem. J.* **1992**, *284*, 539.

13. Holmes, C. F. B.; Luu, H. A.; Carrier, F.; Schimtz, F. J. *FEBS Lett.* **1990**, *270*, 216.

14. Matsumori, N.; Murata, M.; Tachibana, K. *Tetrahedron* **1995**, *51*, 12229.

15. MacKintosh, C.; Klumpp, S. *FEBS Lett.* **1990**, *277*, 137.

16. Nishiwaki-Matsushima, R.; Fujiki, H.; Harada, K.-i.; Taylor, C.; Quinn, R. J. *Bioorg. Med. Chem. Lett.* **1992**, *2*, 673.

17. Kato, Y.; Fusetani, N.; Matsunaga, S.; Hashimoto, K. *J. Am. Chem. Soc.* **1986**, *108*, 2780.

18. Goldberg, J.; Huang, H.-B.; Kwon, Y.-G.; Greengard, P.; Nairn, A. C.; Kuriyan, J. *Nature (London)* **1995**, *376*, 745.

19. Egloff, M.-P.; Cohen, P. T. W.; Reinemer, P.; Barford, D. *J. Biol. Chem.* **1995**, *254*, 942.

20. Huang, H.; Horiuchi, A.; Goldberg, J.; Greengard, P.; Nairn, A. C. *Proc. Natl Acad. Sci.* **1997**, *94*, 3530.

21. Carrell, C. J.; Carrell, H. L.; Erlebacher, J.; Glusker, J. P. *J. Am. Chem. Soc.* **1988**, *110*, 8651.

22. Zhang, Z.; Zhao, S.; Long, F.; Zhang, L.; Bait, G.; Shima, H.; Nagao, M.; Lee, E. Y. C. *J. Biol. Chem.* **1994**, *269*, 16997.

23. Bagu, J. R. *Nature Struct. Biol.* **1995**, *2*, 114.

24. Bagu, J. R.; Sykes, B. D.; Craig, M. M.; Holmes, C. B. *J. Biol. Chem.* **1997**, *272*, 508. Exception: this is a recent modeling paper published after submission of this study which also takes into account Kuriyan's X-ray coordinates as a basis for docking several okadaic acid class inhibitors with PP1.

(*Received in U.S.A.* 21 *February* 1997; *accepted* 30 *June* 1997)